OFFICE OF NAVAL RESEARCH

Contract No. N00014-91-J-1409

Technical Report No. 116

Role of the Double-Layer Cation on the Potential-Dependent Stretching Frequencies and Binding Geometries of Carbon Monoxide at Platinum-Nonaqueous Interfaces

by

Joseph D. Roth and Michael J. Weaver

Prepared for Publication

in

Langmuir

Purdue University

Department of Chemistry

West Lafayette, Indiana 47907

February 1992

CURITY CLASSIFICATION OF THIS PAGE

REPORT DOCUMENTATION PAGE

Form Approved
OMB No. 0704-0188

a. REPORT SECURITY CLASSIFICATION Unclassified	1b. RESTRICTIVE MARKINGS
a. SECURITY CLASSIFICATION AUTHORITY	3. DISTRIBUTION/AVAILABILITY OF REPORT Approved for public release and sale; its distribution is unlimited.
b. DECLASSIFICATION/DOWNGRADING SCHEDULE	
. PERFORMING ORGANIZATION REPORT NUMBER(S) Technical Report No. 116	5. MONITORING ORGANIZATION REPORT NUMBER(S)
a. NAME OF PERFORMING ORGANIZATION Purdue University Department of Chemistry 6b. OFFICE SYMBOL (If applicable)	7a. NAME OF MONITORING ORGANIZATION Division of Sponsored Programs Purdue Research Foundation
c. ADDRESS (City, State, and ZIP Code) Purdue University Department of Chemistry West Lafayette, IN 47907	7b. ADDRESS (City, State, and ZIP Code) Purdue University West Lafayette, IN 47907
a. NAME OF FUNDING/SPONSORING ORGANIZATION Office of Naval Research 8b. OFFICE SYMBOL (If applicable)	9. PROCUREMENT INSTRUMENT IDENTIFICATION NUMBER Contract No. N00014-91-J-1409
c. ADDRESS (City, State, and ZIP Code) 800 N. Quincy Street Arlington, VA 22217	10. SOURCE OF FUNDING NUMBERS PROGRAM ELEMENT NO. / PROJECT NO. / TASK NO / WORK UNIT ACCESSION NO.

1. TITLE (Include Security Classification) Role of the Double-Layer Cation on the Potential-Dependent Stretching Frequencies and Binding Geometries of Carbon Monoxide at Platinum-Nonaqueous Interfaces

2. PERSONAL AUTHOR(S)
Joseph D. Roth and Michael J. Weaver

3a. TYPE OF REPORT	13b. TIME COVERED	14. DATE OF REPORT (Year, Month, Day)	15. PAGE COUNT
Technical	FROM _____ TO _____	February 28, 1992	

6. SUPPLEMENTARY NOTATION

7. COSATI CODES		
FIELD	GROUP	SUB-GROUP

18. SUBJECT TERMS (Continue on reverse if necessary and identify by block number)
influences of the double-layer cation upon the electrode potential-dependent infrared spectral properties of saturated CO adlayers, infrared spectra in alkali metal electrolytes.

9. ABSTRACT (Continue on reverse if necessary and identify by block number)

The influences of the double-layer cation upon the electrode potential-dependent infrared spectral properties of saturated CO adlayers on polycrystalline platinum have been examined in acetonitrile, methanol, tetrahydrofuran (THF), and dichloromethane. These solvents were chosen so to yield a range of dielectric and solvating environments. Two classes of electrolytes were examined, containing tetraalkylammonium and alkali metal cations. For each solvent containing the former electrolytes, near-exclusive terminal CO coordination was observed throughout the accessible potential range (from ca −2.5 to 1 V vs ferrocenium-ferrocene), as evidenced by a single potential-dependent C–O stretching band at ca 2040–2090 cm^{-1}. The ν_{co} frequency-potential slopes depend significantly on the size of the tetraalkylammonium cation. This dependence is approximately consistent with the expectations of a simple double-layer model featuring a linear potential drop throughout the inner layer, with the position of the outer Helmholtz plane being determined by the CO adlayer thickness

0. DISTRIBUTION/AVAILABILITY OF ABSTRACT	21. ABSTRACT SECURITY CLASSIFICATION	
☐ UNCLASSIFIED/UNLIMITED ☐ SAME AS RPT. ☐ DTIC USERS		
2a. NAME OF RESPONSIBLE INDIVIDUAL	22b. TELEPHONE (Include Area Code)	22c. OFFICE SYMBOL

D Form 1473, JUN 86 *Previous editions are obsolete.* SECURITY CLASSIFICATION OF THIS PAGE

(19. cont.)

plus the unsolvated cation radius. The infrared spectra in alkali metal (Li^+, Na^+, K^+) electrolytes yielded a similar terminal ν_{co} feature, which is, however, replaced entirely at relatively negative potentials by a band at ca 1730–1800 cm^{-1}. This effect is ascribed to a potential-induced conversion from terminal to multifold CO coordination geometries, driven by Lewis acid-base interactions between the partly desolvated alkali cations and the CO adlayer. Analogies are noted with cation-induced coordination shifts in polynuclear carbonyl complexes.

ABSTRACT

The influences of the double-layer cation upon the electrode potential-dependent infrared spectral properties of saturated CO adlayers on polycrystalline platinum have been examined in acetonitrile, methanol, tetrahydrofuran (THF), and dichloromethane. These solvents were chosen so to yield a range of dielectric and solvating environments. Two classes of electrolytes were examined, containing tetraalkylammonium and alkali metal cations. For each solvent containing the former electrolytes, near-exclusive terminal CO coordination was observed throughout the accessible potential range (from ca -2.5 to 1 V vs ferrocenium-ferrocene), as evidenced by a single potential-dependent C-O stretching band at ca 2040-2090 cm^{-1}. The ν_{co} frequency-potential slopes depend significantly on the size of the tetraalkylammonium cation. This dependence is approximately consistent with the expectations of a simple double-layer model featuring a linear potential drop throughout the inner layer, with the position of the outer Helmholtz plane being determined by the CO adlayer thickness plus the unsolvated cation radius. The infrared spectra in alkali metal (Li^+, Na^+, K^+) electrolytes yielded a similar terminal ν_{co} feature, which is, however, replaced entirely at relatively negative potentials by a band at ca 1730-1800 cm^{-1}. This effect is ascribed to a potential-induced conversion from terminal to multifold CO coordination geometries, driven by Lewis acid-base interactions between the partly desolvated alkali cations and the CO adlayer. Analogies are noted with cation-induced coordination shifts in polynuclear carbonyl complexes.

INTRODUCTION

Understanding the manner in which the surface electrostatic environment, as determined by the electrode potential, the double-layer ions, and the solvent, influences the properties of adsorbates at metal-solution interfaces constitutes an issue of basic importance in electrochemistry. Most experimental information on this topic has been obtained traditionally by means of potential-dependent surface tension, double-layer capacitance, and related electrochemical measurements.[1] More recently, such thermodynamic information has been supplemented increasingly by a myriad of surface spectroscopic techniques.[2] Of the latter, vibrational spectral methods can yield valuable insight into the various influences of the double-layer environment upon adsorbate surface binding and related properties.

Examining the dependence of vibrational frequencies upon the electrode potential, in particular, constitutes an often-utilized tactic for exploring such effects. A complication that is commonly (if tacitly) faced in such measurements is that the adsorbate coverage and/or bonding configuration, and hence adsorbate-adsorbate and related interactions, vary with the electrode potential. It is therefore desirable to select adsorbate probes and measurement conditions where such potential-induced compositional alterations are minimized. The simplest (if not the ideal) tactic for fulfilling this objective is to select an adsorbate which is bound sufficiently strongly so to yield near-saturated, and hence an effectively constant, surface coverage as the electrode potential and other parameters are altered.

The premier adsorbate that both fulfills this purpose and is especially suitable for infrared spectral measurements is carbon monoxide. The latter virtues derive not only from the high infrared absorbance of the C-O stretching (ν_{co}) vibration, but also from the high sensitivity of the ν_{co} frequency to both

the electrostatic and chemical environment. Not surprisingly, since the inception of surface infrared spectroscopy applied to in-situ electrochemical interfaces there have been numerous studies of potential-dependent ν_{co} spectra, chiefly at polycrystalline p. .tinum-aqueous interfaces.[3] A major restriction of aqueous media for the above purposes, however, is that the accessible potential ranges are limited severely by cathodic hydrogen evolution and CO electrooxidation. The use of selected nonaqueous media can be highly advantageous in this regard since both these potential-limiting processes can essentially be eliminated under anhydrous conditions.

Several reports of potential-dependent infrared spectra for CO adsorbed at metal-nonaqueous interfaces have appeared recently.[4-8] These include studies at single-crystal platinum and rhodium surfaces[6,7] as well as polycrystalline platinum.[4,5,8] Some of these data demonstrate the feasibility of examining the infrared properties of adsorbed CO at near-saturated coverages in quantitative detail over wide (up to ca 5 V) potential ranges. Given this favorable situation, it is of interest to examine in detail the combined influences of the double-layer ionic and solvating environment on the potential-dependent ν_{co} properties of saturated CO adlayers. Recent work from our laboratory has shown that while the nature of the solvent can in some cases exert surprisingly little influence, significant or even dramatic changes in the potential-dependent ν_{co} frequencies and CO binding sites can be observed that are specific to the supporting electrolyte cation.[5-7]

The present paper reports potential-dependent infrared spectra for saturated CO adlayers on polycrystalline platinum in four nonaqueous solvents - acetonitrile, methanol, tetrahydrofuran (THF), and dichloromethane - as a function of the supporting electrolyte cation. The intention is to discern in more detail how the specific nature of the ionic double layer influences the

chemisorbate electrostatic environment. Although limited by solubility considerations, a series of tetraalkylammonium and alkali metal perchlorate (or hexafluorophosphate) salts were employed. The findings demonstrate the importance of nonspecific size affects in the former case and specific CO–interaction effects in the latter examples.

EXPERIMENTAL SECTION

Most general details of the electrochemical surface infrared measurements are provided in refs. 9–11. The spectrometer was a Bruker/IBM IR 98–4A vacuum Fourier transform instrument, with a helical Globar light source and a liquid nitrogen–cooled narrow–band MCT detector. The spectral resolution was ±4 cm^{-1}. A spectroelectrochemical cell was employed that features a micrometer adjustment of the thin–layer thickness defined by the Pt electrode–CaF_2 window separation, and the provision of forced hydrodynamic flow.[9] While designed primarily with flow–cell applications in mind,[9,11] the latter feature enables solutions to be replaced readily by flushing through the thin layer. The electrode was a 0.9 cm diameter Pt disk. It was polished prior to use with 0.05 μm alumina, using water as a lubricant, and then sonicated for 15 min in the solvent to be used in the upcoming experiment. After mounting the electrode in the infrared cell, cyclic voltammograms were recorded in the appropriate solvent containing only the supporting electrolyte, so to check the possible presence of water and other electroactive impurities. Provided that the voltammetric response was satisfactory, CO–saturated electrolyte was then injected into the cell, and the potential cycled several times through the polarizable region with the solution flowing slowly through the thin layer. This procedure was found to yield consistently saturated (or near–saturated) CO coverages, as deduced from the ensuing infrared spectra (see below). This direct mode of CO adlayer preparation in nonaqueous media, also employed in our earlier studies,[5,6] differs from that

of Pons et al, who resorted to using the dissociative chemisorption of vanadium hexacarbonyl.[4] The latter procedure would appear to suffer from several possible complications, including surface contamination by vanadium carbonyl fragments. (Note also that essentially no dissociative chemisorption of methanol to yield CO on platinum occurs from the anhydrous solvent, unlike the situation in the presence of water.[12])

The solvents used were distilled under an atmosphere of nitrogen from the appropriate desiccant[13]: dichloromethane from P_2O_5, acetonitrile from CaH_2, and THF from potassium metal with benzophenone as an indicator. Methanol was reacted with Mg turnings to remove water *before* distillation. The supporting electrolytes were synthesized as follows. The tetramethylammonium, tetraethylammonium, and tetrabutylammonium perchlorates (TMAP,TEAP,TBAP) were prepared by the metathesis of the appropriate tetraalkylammonium bromide (Aldrich) and perchloric acid (Fisher) in water. The resulting TMAP, TEAP, and TBAP were recrystallized twice from water, or water, and then ethanol, and methanol/water, respectively, and dried at 100°C under vacuum for 24 hours. The corresponding tetraethylammonium and tetrabutylammonium hexafluorophosphates (TEAH,TBAH) were prepared similarly by using ammonium hexafluorophosphate, and recrystallized twice from absolute ethanol. The alkali perchlorates ($LiClO_4$, $NaClO_4$, $KClO_4$, from G.F. Smith) were recrystallized twice from water, and dried at 210°C under vacuum. Potassium hexafluorophosphate (Aldrich) was recrystallized twice from water and dried at 100°C under vacuum.

The electrode potentials were both measured and are quoted here versus the ferrocenium–ferrocene ($Fc^{+/o}$) couple in the same solvent; this involved the use of an equimolar Fc^+/Fc mixture in contact with a Pt wire in a separate reference compartment. The exception is measurements in aqueous media, for which a Ag/AgCl (3M KCl) reference electrode was used. All measurements were made at room

temperature, 23 ± 1°C.

RESULTS

In our earlier preliminary communication on this topic, we noted that nonaqueous solvents containing tetraalkylammonium and alkali metal cations yield dramatically different potential-dependent infrared spectra for saturated CO adlayers on platinum.[5] Specifically, in the former electrolytes a single C-O stretching (ν_{co}) band at ca 2030-2100 cm^{-1}, indicative of terminal (i.e., atop) CO coordination, is observed throughout the accessible ranges of electrode potential (typically from -2.5 to 1 V vs $Fc^{+/o}$). In the latter electrolytes, however, this band is replaced at lower potentials by a ν_{co} feature at markedly lower frequencies, ca 1730-1800 cm^{-1}, indicative of multifold CO coordination. It is therefore convenient to consider the present, more detailed, results obtained in these two classes of supporting electrolytes in sequential fashion.

Tetraalkylammonium Electrolytes

Representative potential-difference infrared (PDIR) spectra in the ν_{co} frequency region for saturated CO adlayers on polycrystalline platinum in tetraalkylammonium electrolytes are displayed in acetonitrile, methanol, dichloromethane, and THF in Figs. 1A, 2, 3A, and 3B, respectively. The bipolar ν_{co} features obtained in most instances reflect the spectral shifts occurring between the pairs of sample and reference potentials chosen to generate the potential-difference absorbance spectra. The oft-utilized PDIR tactic provides a straightforward means of eliminating solvent and other potential-independent spectral interferences. Unlike aqueous media, adsorbed CO is stable throughout the accessible potential range in the present nonaqueous solvents, so that ν_{co} spectral contributions are present at both the sample and reference potentials. (In aqueous solution, CO can usually be arranged to be removed entirely by

electrooxidation at suitably positive potentials, enabling "absolute" ν_{co} spectra, consisting of *unipolar* bands, to be obtained[11,15].)

Two distinct tactics were utilized here to generate PDIR spectra. The first involves acquiring sets of interferograms (typically each 100 scans) at each potential during a staircase ramp through the polarizable potential region. This procedure[14] enables interferogram sets at any two potentials in the sequence to be combined so to yield a PDIR spectrum. The resulting flexibility is an important virtue since the extraction of spectral information at a given potential is facilitated by selecting a "reference" spectrum at a sufficiently different potential so that overlap between the positive- and negative-band components are minimized. The spectra in Figs. 1A, 2A, and 3 were acquired in this manner.

The other PDIR procedure employed here involves modulating the potential repeatedly between a pair of reference and sample potentials (usually every ca 20s, after every 50 interferometer scans), and subtracting the coadded spectral sets as before. This conventional tactic usually offers the advantage of greater sensitivity, which turned out to be significant here for the detection of weak bridging ν_{co} features. The spectra in Figures 1B and 2B were generated in this manner. This procedure offers less flexibility than the former tactic, however, and is rather more time consuming.

The resulting PDIR spectra obtained in tetraalkylammonium electrolytes exhibit a single bipolar band throughout the accessible potential range. This finding, noted in preliminary fashion in ref. 5, applies throughout the wider range of solvents and tetraalkylammonium supporting electrolytes examined in the present study. The largely symmetrical nature of the bipolar band results from the well-known upshifts in the terminal ν_{co} frequency, ν_{co}^{t}, as the potential, E, is increased, along with the retention of a roughly potential-independent site

occupancy. Admittedly, the band tends to broaden towards more negative potentials, as seen in the negative-going PDIR component in Figs. 1A, 2A, and 3A. This broadening, which is absent on monocrystalline platinum surfaces[5,6] probably reflects the occurrence of slightly differing ν_{co}^{t} – E dependencies associated with the inevitable distribution of local bonding environments on polycrystalline platinum.

The commonly observed overlap between the two components of the bipolar PDIR bands can yield sufficient mutual interference to complicate extraction of frequency and related parameters for the band partners. Nevertheless, these effects upon the required peak frequency, ν_{co}^{t}, can be rendered essentially negligible by selecting sufficiently different sample and reference potentials, typically by $\gtrsim$ 0.5 to 1.0 V. These conditions also enable approximate estimates of the integrated band absorbances, A_i, to be obtained. The A_i values (ca 0.05 cm^{-1}) are comparable to those observed within the same optical geometry[16] for saturated CO adlayers on polished polycrystalline platinum in aqueous media, for which the coverage is known to be roughly a monolayer by coulometric means[17]. This observation adds credence to the notion that essentially saturated adlayers are also formed in the present nonaqueous environments.

Given the largely potential-independent CO binding geometry obtained in tetraalkylammonium electrolytes, it is of interest to examine the manner and extent to which the ν_{co}^{t} – E behavior is dependent upon the properties, specifically the size, of the cation. Figures 4–6 contain plots of ν_{co}^{t} versus E for saturated CO adlayers on Pt in acetonitrile, methanol, and THF, respectively, in various tetraalkylammonium supporting electrolytes (open symbols). The most complete data set was obtained in acetonitrile (Fig. 4), for which all four tetraalkylammonium cations (TMA^+, TEA^+, TBA^+, THA^+) could be employed as perchlorate salts, although the concentration of TMAP used (ca 0.05 M) was lower than for

the other electrolytes (0.15 M) due to solubility constraints.

Examination of Fig. 4 shows that the ν_{co}^{t} – E slopes decrease systematically as the cation size increases. Some comparable observations at polycrystalline[8] and single-crystal platinum electrodes[7] in acetonitrile have been reported previously. Roughly similar dependencies of the ν_{co}^{t} – E slopes upon the tetraalkylammonium cation are also observed in methanol and THF (Figs. 5,6), although the data are more limited due to electrolyte solubility restrictions.

Even though most data were obtained in 0.15 M electrolyte, some measurements were made to check the possible dependence of the ν_{co}^{t} – E behavior on the electrolyte concentration. Only small or imperceptible effects were observed, however; thus the ν_{co}^{t} – E slopes in acetonitrile increased by less than ca 5% for TBAP concentrations between 0.02 and 2 M. Also, as might be expected, substitution of perchlorate by hexafluorophosphate for a electrolyte having a given tetraalkylammonium cation made essentially no difference to the ν_{co}^{t} – E behavior.

A summary of $d\nu_{co}^{t}/dE$ values, along with ν_{co}^{t} values obtained at a given electrode potential (0 V vs $Fc^{+/o}$), in the various solvent–tetraalkylammonium electrolyte combinations examined here is given in Table I. In harmony with recent related observations on Pt(111) and Pt(110) in nonaqueous media[6,7], these results show that the ν_{co} – E behavior for saturated CO adlayers, while dependent somewhat on the tetraalkylammonium cation, is insensitive to the solvent medium at a given electrode potential (measured versus a "solvent–insensitive" reference electrode such as $Fc^{+/o}$). We defer discussion of these data, however, until after the results obtained in alkali electrolytes have been considered.

Alkali Metal Electrolytes

Illustrative PDIR spectra for saturated CO adlayers on polycrystalline platinum in acetonitrile and methanol containing 0.15 M $NaClO_4$ are shown in Figs.

1B and 2B, respectively. At potentials positive of ca −0.8 V and −1.1 V in these two solvents, similar spectra were observed as in the tetraalkylammonium electrolytes, featuring a single bipolar feature, indicative of essentially exclusive terminal CO coordination. Comparable findings were also obtained in THF for potentials positive of ca −1.4 V. A summary of ν_{co}^{t} − E data in alkali electrolytes under these conditions is included in Table I. At more negative potentials, however, the terminal band diminishes in intensity and eventually disappears entirely, being replaced by a broad weaker feature at ca 1700–1800 cm^{-1}. As noted above, this observation is indicative of a conversion of the CO adlayer into multifold (chiefly twofold bridging) coordination geometries.

Of interest here is the elucidation of the combined roles of the alkali cation and the solvent in driving such potential-induced adsorbate site conversions. It is therefore desirable to examine PDIR spectra for various solvent-supporting electrolyte combinations. As for the tetraalkylammonium salts, the range of cations examined was limited by solubility factors. The most comprehensive data set was obtained in acetonitrile. Figure 7 shows ν_{co}^{t} − E plots for 0.15 M $LiClO_4$, $NaClO_4$, and KPF_6 in acetonitrile, in comparison with corresponding data in 0.15 M TEAP (open triangles). (Heavier alkali-metal salts were found to be insufficiently soluble in acetonitrile.) Virtually identical ν_{co}^{t} − E behavior is obtained in all four electrolytes at potentials, > −0.6 V, where terminal CO coordination predominates. At more negative potentials, where progressive terminal-bridging site conversion occurs in the alkali electrolytes, the ν_{co}^{t} values fall markedly below the linear ν_{co}^{t} − E line observed in TEAP. These ν_{co}^{t} downshifts are due to diminutions in adsorbate dipole-dipole coupling, associated with the progressive potential-induced decreases in the coverage of terminally bound CO as the adlayer shifts increasingly to bridge bonding.

Interestingly, both the ν_{co}^{t} − E behavior, along with the potential-

dependent intensities of the terminal and bridging ν_{co} bands, are virtually independent of the nature of the alkali metal cation in acetonitrile. The potential-dependent behavior is also insensitive to the electrolyte concentration, although significant (0.2 - 0.3 V) positive shifts in the potential where CO site conversion is initiated could be induced by increasing the cation concentration from 0.02 to 2 M. Comparable behavior was also observed in methanol and THF; ν^t_{co} - E plots obtained with alkali electrolytes in these solvents are included in Figs. 5 and 6, respectively (filled symbols). Some dependence of the potential-induced site conversion on the solvent, however, was observed in that the process occurs at significantly (ca 0.5 - 1.0 V) more negative potentials (versus the $Fc^{+/o}$ electrode) in THF than in methanol and especially acetonitrile.

DISCUSSION

A significant feature of the present findings is that each of the organic cations examined here yields markedly different potential-dependent ν_{co} spectra than those observed in the presence of the alkali cations. Furthermore, and perhaps surprisingly, the former (ν^t_{co} - E dependencies) are sensitive to the nature of the organic cation, whereas the latter more specific effect (potential-induced CO site conversion) is insensitive to the alkali cation. In order to rationalize such disparate phenomena, it is useful to consider the nature of the anticipated electrostatic influences of the double-layer cations upon the inner layer in general, and the CO adlayer in particular.

The observed decreases in the ν^t_{co} - E slopes in the presence of progressively larger tetraalkylammonium cations can be understood most simply in terms of their influence upon the potential profile across the double layer. As the cation radius increases, the outer Helmholtz plane (oHp) should be situated further from the metal surface, so that the fraction of the inner-layer potential

drop lying across the CO adlayer will diminish, so that $d\nu_{co}/dE$ decreases. This model can also account for the convergence of these ν_{co} – E plots at positive potentials, ca 0.5 V vs $Fc^{+/o}$, seen most clearly in acetonitrile (Fig. 4). The potential of zero charge (pzc) is anticipated to be located close to this point, where the potential drop induced by the free (cation) charges will be absent, yielding cation-independent ν_{co} values, as are observed here. (See ref. 6 for a discussion of this point[24]). The potential-induced shifts in ν_{co} frequency have been ascribed to changes in the local electrostatic field (first-order Stark effect)[19] and to potential-dependent metal-CO bonding.[20] Both these models predict that the ν_{co} frequency will be dependent on the potential drop across the CO layer, so that no demarcation between them can be made on the basis of the present observations.

Nevertheless, it is of interest to compare the present cation-dependent ν^t_{co} – E slopes with the expectations of a simple double-layer model based on cation size. Estimates of the effective "hard-sphere" radius, r_{hs}, of the tetraalkylammonium cations can be estimated from values for the analogous star alkanes as described in ref. 21, involving corrections to van der Waals radii as given in ref. 22. The resulting r_{hs} estimates are: TMA^+, 2.83Å; TEA^+, 3.38Å; TBA^+, 4.22Å; and THA^+, 5.05Å. While these values are slightly larger than the crystallographic radii[23], the variations with cation size are closely similar. The simplest double-layer model assumes that the potential drops linearly between the metal surface and the oHp, i.e., the inner-layer field is constant. We anticipate that the inner-layer thickness equals $d_{co} + r_{hs}$, where d_{co} is the distance across the CO adlayer (taken here as 3.5Å). Given that the ν_{co} frequency presumably senses only the potential drop across d_{co}, from simple geometry we can write

$$(d\nu^t_{co}/dE)^{-1} = [(d\nu^t_{co}/dE)^{-1}_{r=0}](d_{co} + r_{hs})/d_{co} \quad (1a)$$

$$= K(d_{co} + r_{hs}) \quad (1b)$$

where K is a constant. The first term on the right-hand-side is the inverse ν_{co}^{t} - E slope anticipated in the limit where $r_{hs} = 0$, i.e., where the entire inner-layer potential drop is located across the CO adlayer.

It should be noted that this treatment neglects the influence of the diffuse double-layer on the ν_{co}^{t} - E slope. Evidence that this contribution is unlikely to be important is deduced from the observation that $d\nu_{co}^{t}/dE$ is essentially independent of ionic strength (from 0.02 to 2 M). Estimates of $d\phi_d/dE$ in the appropriate electrode potential ranges, where ϕ_d is the potential across the diffuse layer, were obtained from Gouy-Chapman theory combined with the measured inner-layer capacitance for the CO-covered Pt surface in acetonitrile, $6(\pm 1)\mu F\ cm^{-2}$[25]. The resulting $d\phi_d/dE$ estimates varied from about 0.07 at 0.02 M to 0.035 at 2 M ionic strength. On this basis, we anticipate that the presence of the diffuse-layer potential should diminish $d\nu_{co}^{t}/dE$ only to a small extent, by roughly a few percent, and can be neglected here.

Another possible complication is that the concentrations of free ions in the non-polar solvents dichloromethane and THF will be markedly below the corresponding formal values as a consequence of ion pairing. This factor is unlikely to affect greatly the present results, however, since the cation concentration at the oHp will be determined largely by the electronic charge density on the metal surface. Indeed, this assertion is supported by the close similarly in the results obtained here irrespective of the solvent permittivity.

Equation (1) suggests that a plot of $(d\nu_{co}^{t}/dE)^{-1}$ versus the inner-layer thickness $(d_{co} + r_{hs})$ should yield a straight line passing through the origin. Figure 8 shows such a plot for the ν_{co}^{t} - E data obtained in acetonitrile (circles), methanol (squares), and THF (triangles). While the scatter in the data, at least for the latter two solvents, make the extrapolations of dubious quantitative validity, it is nonetheless interesting to note that the x-

intercepts are fairly small, ca 2Å. The intercepts are smaller, about 1Å, if crystallographic radii are employed for r_{hs}. The residual x-intercepts may reflect the presence of smaller inner-layer thicknesses than estimated here, perhaps due to the cations being situated partly between CO adlayer molecules, alternatively, they may well signal a limitation of the simple "constant-field" (and average potential) model itself.

Nonetheless, on this basis the slopes of the plots in Fig. 8 enable approximate estimates to be obtained of the so-called "Stark-tuning rate" expressed in terms of the electric field $\mathscr{E}$ across the CO adlayer rather than the electrode potential E. The former quantity, $d\nu_{co}/d\mathscr{E}$ ($cm^{-1}/V\ cm^{-1}$), has been evaluated in corresponding field-dependent measurements at metal-ultrahigh-vacuum (uhv) interfaces by Lambert and coworkers[19,26]. The $(d\nu^{t}_{co}/d\mathscr{E})$ values extracted in this manner from Fig. 8, 1.0 (± 0.2) x 10^{-6} $cm^{-1}/V\ cm^{-1}$, are fourfold larger than the value reported for a near-saturated CO adlayer on Pt(111) in uhv[26]. A similar disparity between electrochemical and Pt(111)-uhv "Stark tuning rates" has been noted previously using data obtained for the Pt(111)-aqueous interface[27]. One difference between the electrochemical and uhv systems is that the fields generated across the CO adlayers in the former are much (ca 10^3 fold) larger. In addition, the fraction of the total applied potential drop located across the CO adlayer is large (≳ 50%) in the electrochemical systems, but very small in the uhv environment. This latter consideration makes the resulting $d\nu^{t}_{co}/d\mathscr{E}$ estimates obtained for the metal-uhv systems more susceptible to errors arising from nonuniform field gradients. This interesting issue is pursued further elsewhere, in connection with $d\nu^{t}_{co}/d\mathscr{E}$ data obtained at monocrystalline metal-solution interfaces[7].

We consider now the likely factors responsible for the potential-induced CO site conversions observed in alkali metal electrolytes. Some guidance can be

obtained from a perusal of the literature on ion-pairing effects involving transition-metal carbonyl anions in nonaqueous media[28]. A variety of cations, including alkali metal ions, have been shown to interact specifically (in a Lewis acid-base sense) with the oxygen of the coordinated CO in such complexes. Such interactions can be reflected in significant downshifts of the carbonyl ν_{co} frequency[28b]. Further, dissolved cations are known to shift CO coordination from terminal to bridging geometries in some polynuclear carbonyls[28a,29].

These phenomena can be understood in terms of the polarization of negative charge on the CO ligand induced by cation association. This polarization, presumably yielding greater metal-CO back bonding, should decrease the ν_{co} frequency, as observed. The greater degree of metal-CO back bonding occurring for bridging carbonyl geometries, reflected in the markedly (150-200 cm^{-1}) lower ν_{co} frequencies compared with terminal coordination, should enhance the degree of carbonyl-cation interactions. Conversely, then, the observed tendency of cations (Lewis acids) to induce shifts from terminal to bridging coordination can be understood in terms of the additional carbonyl-cation stabilization thus induced. The driving force for this coordination geometry change will be enhanced towards more negative potential from the greater electrostatic interactions between the cation and the metal surface.

On this basis, then, the observed disappearance of the terminal ν_{co} band and its replacement by a feature at markedly (200-250 cm^{-1}) lower frequencies in the presence of alkali cations at negative potentials (Figs. 1B,2B) can be ascribed to a terminal-bridging CO site conversion induced by short-range electrostatic interactions between the cations and the CO adlayer. Nonetheless, given that significant ν_{co} frequency downshifts for metal carbonyls can be induced by solution cations *in the absence* of such changes in coordination geometry (vide supra), this site-conversion interpretation might appear

questionable.

The present results, however, favor its validity. Thus large cation concentrations should be present at the oHp throughout the potential ranges examined here, which are uniformly below the pzc (ca 0.8 V vs $Fc^{+/o}$[24]). Nevertheless, the terminal CO band observed over a substantial portion of the accessible potential range in alkali cation electrolytes exhibits ν_{co} frequencies which are closely similar, or even higher, than those observed for larger tetraalkylammonium cations (see Figs. 5–7). Consequently, then, there is no evidence of significant alkali cation–induced downshifts in ν_{co} frequency within the terminal CO adlayer geometry.

Furthermore, the observed potential–induced replacement of the usual terminal CO feature by an entirely separate, lower–frequency, band is by itself indicative of a sharp alteration in site occupancy. The site conversion will be driven progressively towards more negative potentials by the greater electrostatic interactions between the double–layer cations and the increasingly negative charge density on the metal surface. This interpretation is also supported by the sharp downshifts in the terminal ν_{co} frequencies that accompany the decreases in band intensity towards more negative potentials (Figs. 5–7). A shift in site occupancy towards bridging coordination will diminish the dynamic dipole coupling associated with interactions between terminally bound CO adsorbates, thereby downshifting ν_{co}^{t}[11].

Nevertheless, a perhaps unexpected feature of the present results is the insensitivity of the details of the potential–induced site conversion, including the ν_{co} frequency–potential behavior, to the size of the alkali cation (compare Li^+, Na^+, K^+ in Fig. 5). This finding, however, can be rationalized in terms of the generalized potential–dependent equilibrium expressed as

$$Pt\text{–}CO + M^+(solv) \rightleftharpoons Pt\text{–}CO\ldots M^+ \qquad (2)$$

where M^+(solv) refers to a solvated alkali cation present at the oHp. While Li^+ constitutes a stronger Lewis acid than K^+, for example, the former cation should be more tightly solvated, even at the oHp. Consequently, the specific interaction with the CO adlayer presumably required for site conversion, while intrinsically more favorable for Li^+ in view of its smaller radius, will be counteracted by the greater energy cost required to partly desolvate the cation. In other words, the equilibrium in Eq(2) can be perceived as a competition for M^+ coordination sites between the solvent and the CO adlayer.

Also consistent with this picture is the observation that the terminal-bridge site conversion proceeds at significantly (ca 0.5 - 1 V) more negative potentials in THF than in methanol and acetonitrile. The greater basicity of THF compared with the other solvents should yield a higher energy for partial desolvation of the alkali cation, thereby requiring that more negative potentials (and hence higher negative electrode charges) be attained in order to induce CO site conversion. For the tetraalkylammonium cations, the carbon linkages provide a covalent "solvation" of the ion, thereby preventing the positive charge from interacting specifically with the CO adlayer so to induce site conversion even at the most negative potentials, ca -2.5 V vs $Fc^{+/o}$, examined here.

CONCLUDING REMARKS

The present results show that the nature of the double-layer cation can exert profound influences upon the CO adlayer structure and properties, arising from both nonspecific and specific electrostatic interactions. Despite their significance, such effects have been reported previously only rarely, although Anderson and Huang have recently examined the influence of tetraalkylammonium ion size on ν^t_{co} - E behavior in acetonitrile[8]. The absence of such documented effects in the aqueous media commonly employed for electrochemical infrared studies can be ascribed to the smaller potential ranges accessible in water,

together with the stronger solvation of alkali metal cations and the insolubility of most tetraalkylammonium salts. While some differences are noted between ν_{CO} spectra obtained for CO adlayers on Pt in neutral alkali electrolytes compared with $HClO_4$ or H_2SO_4[31], they are ascribably largely to the differing ranges of electrode potential that are accessible in these media[32]. More significant alkali cation effects in aqueous media, however, have been observed for thiocyanate adsorption on platinum by means of infrared spectroscopy[33].

It is worth commenting specifically on the present results in relation to the potential-dependent CO binding geometries observed on monocrystalline platinum and rhodium electrodes in aqueous[27,32] as well as nonaqueous media[6,7]. In large part, the shifts in CO site occupancy from terminal to bridging coordination seen at some of these ordered metal-aqueous systems[27,32] occur at markedly higher (i.e., less negative) potentials than the alkali cation-induced effects observed in the present work. The former site conversions have been interpreted in terms of the nonspecific effects of electrode potential, with attendant variations in electrode charge and the double-layer field[27,32]. Consideration of such surface potential effects upon CO adlayers has enabled some understanding to be reached of the differing behavior of ordered metal surfaces in related electrochemical and uhv systems[27,32]. Some more specific effects of the double-layer environment upon these systems, however, have been observed, primarily at lower CO coverages where solvent and/or hydrogen coadsorption can play a role[27,32].

For Pt(111) in aqueous $NaClO_4$ electrolytes, extensive terminal-bridging site conversion for saturated CO adlayers does not occur within the accessible potential region[32]. Nevertheless, such site conversion is observed for Pt(111) in acetonitrile/0.1 M $NaClO_4$ at potentials negative of ca -0.8 V vs $Fc^{+/o}$; the corresponding transition on Pt(110) occurs at ca -1.3 V[7]. These observations on

monocrystalline Pt surfaces are closely related to the present findings on polycrystalline platinum. The similarities also extend to the ν_{co}^{t} - E dependencies observed in tetraalkylammonium electrolytes[6,7]. Further discussion of these issues, along with a comparison with related metal-uhv systems, will be given elsewhere[7].

ACKNOWLEDGMENT

This work is supported by the National Science Foundation and the Office of Naval Research.

REFERENCES

1. See for example: Bockris, J.O'M.; Conway, B.E.; Yeager, E., eds., "Comprehensive Treatise of Electrochemistry", Vol. 1, Plenum, New York, 1980, especially Chapters 1,2,4, and 8

2. See for example, reviews in: Compton, R.G.; Hamnett, A., eds., "Comprehensive Chemical Kinetics", Vol. 29, Elsevier, Amsterdam, 1989

3. For example, see overview in: Christensen, P.A.; Hamnett, A., in ref. 2, Chapter 1

4. (a) Anderson, M.R.; Blackwood, D.; Pons, S., J. Electroanal. Chem., **1988**, 256, 387; (b) Anderson, M.R.; Blackwoood, D.; Richmond, T.G.; Pons, S., J. Electroanal. Chem., **1988**, 256, 397; (c) Russell, A.E.; Pons, S.; Anderson, M.R., Chem. Phys., **1990**, 141, 41; (d) Russell, A.E.; Blackwood, D.; Anderson, M.R.; Pons, S., J. Electroanal. Chem., **1991**, 304, 219

5. Roth, J.D.; Chang, S.-C.; Weaver, M.J., J. Electroanal. Chem., **1990**, 288, 285

6. Chang, S.-C.; Jiang, X.; Roth, J.D.; Weaver, M.J., J. Phys. Chem., **1991**, 95, 5378

7. Jiang, X.; Weaver, M.J., Surface Sci., submitted

8. Anderson, M.R.; Huang, J., J. Electroanal. Chem., in press

9. Roth, J.D.; Weaver, M.J., J. Electroanal. Chem., **1991**, 307, 119

10. Chang, S.-C.; Weaver, M.J., J. Chem. Phys., **1990**, 92, 4582

11. Roth, J.D.; Weaver, M.J., Anal. Chem., **1991**, 63, 1603

12. Gao, P.; Chang, S.-C.; Zhou, Z.; Weaver, M.J., J. Electroanal. Chem., **1989**, 272, 161

13. Mann, C.K., in "Electroanalytical Chemistry – A Series of Advances", Bard, A.J., ed, Vol. 3, Marcel Dekker, New York, 1969, p.57

14. This tactic is a variant of the so-called "single potential alteration infrared" (SPAIR) technique, whereby potential-difference spectra are acquired without repeated potential modulation[15]

15. Corrigan, D.S.; Leung, L.-W.H.; Weaver, M.J., Anal. Chem., **1987**, 59, 2252

16. One should note that such A_i values are dependent upon the particular thin-layer optical geometry employed. Thus ca 3-fold larger A_i values are obtained in our laboratory when a bevelled CaF_2 window is employed, rather than a flat window as used in the present flow-cell arrangement. (The former is utilized in our surface infrared studies at monocrystalline electrodes[11].) These variations arise chiefly from differences in the effective angle of incidence of the p-polarized infrared light on the metal surface, and the resultant differences in the electromagnetic field intensity[18].

17. Chang, S.-C.; Roth, J.D.; Weaver, M.J., Surface Sci., **1991**, 244, 113

18. For example, see: Seki, H.; Kunimatsu, K.; Golden, W.G., Appl. Spect., **1985**, 39, 437

19. For example: Lambert, D.K., J. Chem. Phys., **1988**, 89, 3847, and references therein.

20. Anderson, A.B., J. Electroanal. Chem., **1990**, 280, 37

21. Ben-Amotz, D.; Herschbach, D.R., J. Phys. Chem., **1990**, 94, 1038

22. Bondi, A., J. Phys. Chem., **1964**, 68, 441

23. For example, see: Nightingale, Jr., E.R., J. Phys. Chem., **1959**, 63, 1381

24. Note that the aqueous saturated calomel electrode (SCE) utilized in ref. 6 has a potential of about -0.3 V on the $Fc^{+/o}$ scale in the nonaqueous media used here. Thus, the convergence point for the ν_{co} - E plots for polycrystalline Pt in acetonitrile is about 0.8 V vs SCE. A similar intersection potential has been observed for Pt(110) in this media[7], and a slightly higher (ca 1.0 V vs SCE) value for Pt(111)[6]. This difference can be understood from the lower work functions, and hence pzc values, expected for polycrystalline Pt and Pt(110) compared with Pt(111). The issue will be explored further in ref. 7.

25. This value was obtained by means of a.c. impedance measurements.

26. Luo, J.-S.; Tobin, R.G.; Lambert, D.K.; Wagner, F.T.; Moylan, T.E., J. Electron. Spectrosc. Relat. Phenom., **1990**, 54/55, 469

27. Chang, S.-C.; Weaver, M.J., J. Phys. Chem., **1991**, 95, 5391

28. See for example: (a) Shriver, D.F., J. Organomet. Chem., **1975**, 94, 259;

(b) Darensbourg, M.Y., Prog. Inorg. Chem., **1985**, 33, 221

29. For example: (a) Alich, A.; Nelson, N.J.; Strope, D.; Shriver, D.F., Inorg. Chem., **1972**, 11, 2976; (b) Adams, H-N.; Fachinetti, G.; Strähle, J., Angew. Chem. (Int. Ed.), **1980**, 19, 404

30. For example: Chang, S.-C.; Weaver, M.J., Surface Sci., **1990**, 230, 222

31. Tornquist, W.; Giullaume, F.; Griffin, G.L., Langmuir, **1987**, 3, 477

32. Chang, S.-C.; Weaver, M.J., Surface Sci., **1990**, 238, 142

33. Ashley, K.; Samant, M.G.; Seki, H.; Philpott, M.R., J. Electroanal. Chem., **1989**, 270, 349

TABLE I Summary of ν_{co} Frequency-Electrode Potential Slopes, $d\nu^t_{co}/dE$, for Polycrystalline Pt in Nonaqueous Media Containing Various Supporting Electrolytes

Solvent	Electrolyte[a]	$\nu^t_{co}(cm^{-1})$ at 0 V vs $Fc^{+/o}$	Potential range[c] V vs $Fc^{+/o}$	$d\nu^t_{co}/dE$[d] $cm^{-1}\ V^{-1}$
Acetonitrile	0.15 M THAP	2085	0.9 to −2.5	16.9
	0.15 M TBAP	2083	0.8 to −2.4	19.3
	0.15 M TEAP	2082	0.9 to −2.4	22.5
	ca 0.05 M TMAP	2081	0.8 to −2.0	26.2
	0.15 M $LiClO_4$	2083	0.6 to −0.6	22.1
	0.02 M $NaClO_4$	2081	0.8 to −0.9	21.0
	0.15 M $NaClO_4$	2082	0.7 to −0.7	21.9
	2.0 M $NaClO_4$	2082	0.8 to −0.7	22.1
	0.15 M KPF_6	2084	1.0 to −0.5	23.8
Methanol	ca 0.1 M THAP	2081	0.8 to −1.6	17.5
	0.15 M TBAP	2080	0.6 to −1.8	18.5
	ca 0.1 M TEAP	2080	0.4 to −1.6	24.0
	0.15 M $NaClO_4$	2081	0.6 to −0.6	18.9
THF	0.15 M THAP	2089	0.6 to −2.8	15.9
	0.15 M TBAP[b]	2088	0.8 to −2.6	16.5
	0.01 M TEAH	2083	0.6 to −2.4	21.3
	0.15 M $LiClO_4$	2087	0.8 to −1.2	17.5
Dichloromethane	0.15 M THAP	2087	1.0 to −2.1	15.6
	0.30 M TBAP	2080	1.4 to −1.8	22.0
Water	0.15 M TEAP	2075[e]	0.0 to −0.8[e]	25.0

[a] THA = tetraheptylammonium; TBA = tetrabutylammonium; TEA = tetraethylammonium; TMA = tetramethylammonium; P = perchlorate; H = hexafluorophosphate. Approximate concentrations given refer to saturated values.

[b] Solution also contained 50 mM TBAH so to decrease resistivity.

[c] Potential range over which $d\nu^t_{co}/dE$ value given in adjacent right-hand column refers.

[d] Values given typically were reproducible to within $\pm 0.2\ cm^{-1}\ V^{-1}$.

[e] Values obtained using aqueous Ag/AgCl(sat KCl), assuming that $Fc^{+/o}$ electrode potential is 0.2 V on this scale.

FIGURE CAPTIONS

Fig. 1

Sets of potential-difference infrared (PDIR) absorbance spectra in ν_{CO} frequency region for CO adlayers on polycrystalline Pt in CO-saturated acetonitrile containing (A) 0.15 M THAP and (B) 0.15 M $NaClO_4$. The sample potentials in each PDIR spectrum are as indicated (vs $Fc^{+/o}$). The spectra in (A) were collected with the potential altered in a staircase fashion, 100 interferometer scans being collected at each (sample) potential; the reference spectrum was obtained at 0.80 V. For (B), the potential was modulated between the sample and reference (0.49 V) values every 50 scans, a total of 250 scans being collected.

Fig. 2

Sets of PDIR spectra for CO adlayers on polycrystalline Pt in CO-saturated methanol containing (A) 0.15 M TMAP and (B) 0.15 M $NaClO_4$. The sample potentials are as indicated (vs $Fc^{+/o}$). The spectra were collected as in Fig. 1A; the reference spectra were obtained at 0.10 V.

Fig. 3

Sets of PDIR spectra for CO adlayers on polycrystalline Pt in (A) dichloromethane and (B) THF. Both CO-saturated solvents contained 0.15 M THAP. The sample potentials are as indicated (vs $Fc^{+/o}$). The spectra were collected as in Fig. 1A; the reference spectra in (A) and (B) were obtained at -2.0 and -1.60 V, respectively.

Fig. 4

Plots of the terminal C-O stretching frequency, ν^{t}_{CO}, versus electrode potential for a saturated CO adlayer in acetonitrile containing various tetraalkylammonium perchlorate electrolytes. Key: 0.15 M THAP, circles; 0.15 M TBAP, squares; 0.15 M TEAP, upright triangles; saturated (ca 0.05 M) TMAP, inverted triangles.

Fig. 5

As for Fig. 4, but in CO-saturated methanol. Key: saturated (ca 0.1 M) THAP, circles; 0.15 M TBAP (open squares), saturated (ca 0.1 M) TEAP (triangles); 0.15 M $NaClO_4$ (closed squares).

Fig. 6

As for Fig. 4, but in CO-saturated THF. Key: 0.15 M THAP, open circles; 0.15 M TBAP, open squares; saturated (ca 0.01 M) TEAH + 50 mM TBAH, triangles; 0.15 M $LiClO_4$, filled circles; 0.15 M $NaClO_4$.

Fig. 7

Comparison between ν_{co}^{t} – E plots for saturated CO adlayer in acetonitrile using 0.15 M TEAP (triangles) and alkali salts as electrolytes: 0.15 M $LiClO_4$, open circles; 0.15 M $NaClO_4$, filled circles; 0.15 M KPF_6, open squares.

Fig. 8

Plots of inverse "Stark tuning rate", $(d\nu_{co}^{t}/dE)^{-1}$, measured in various tetraalkylammonium electrolytes (Table I) versus estimated inner-layer thickness (see text) in acetonitrile (circles), THF (triangles), and methanol (squares).

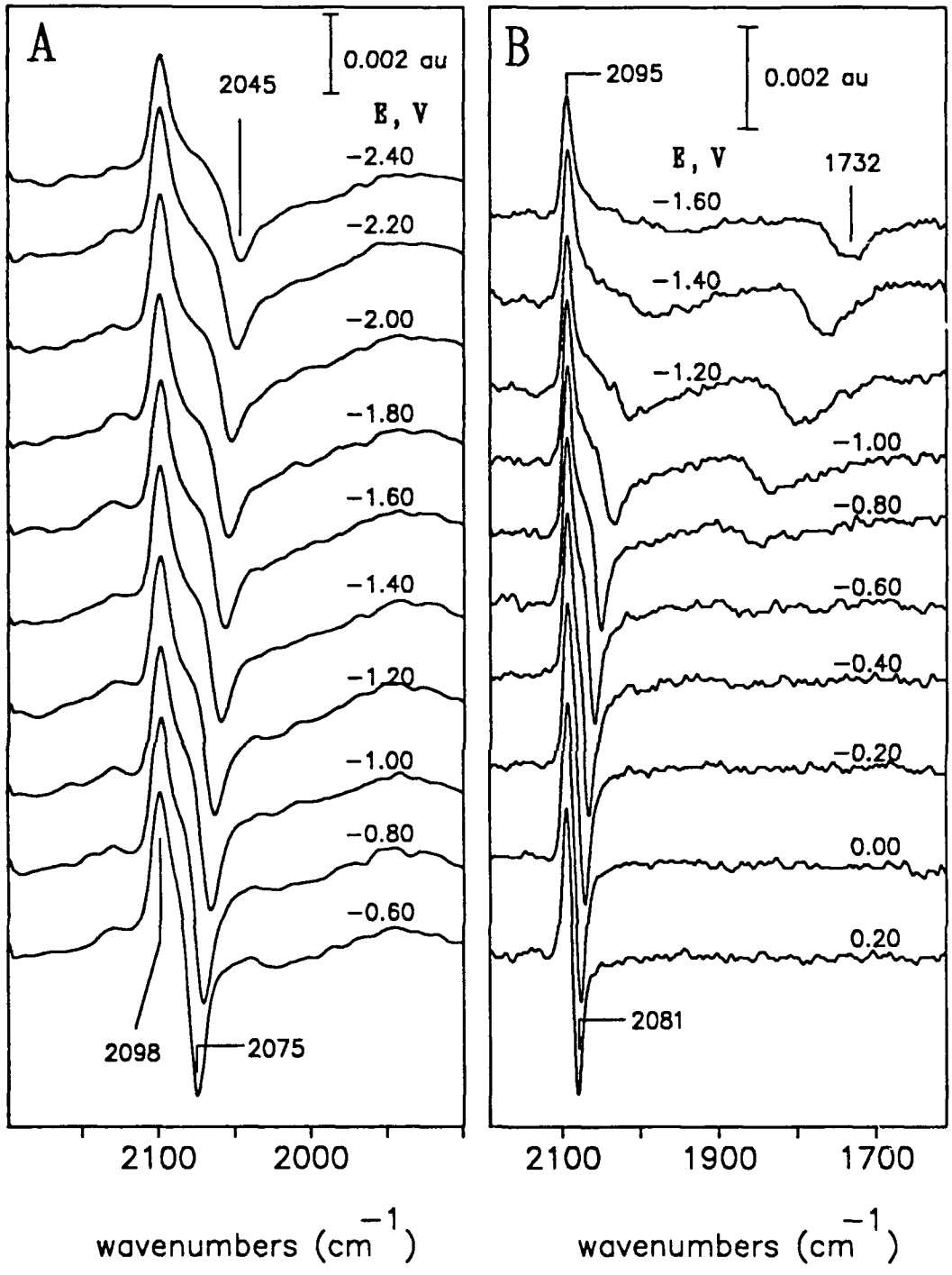
A
0.002 au
2045
E, V
−2.40
−2.20
−2.00
−1.80
−1.60
−1.40
−1.20
−1.00
−0.80
−0.60
2098
2075
2100
2000
wavenumbers (cm−1)
B
2095
0.002 au
E, V
1732
−1.60
−1.40
−1.20
−1.00
−0.80
−0.60
−0.40
−0.20
0.00
0.20
2081
2100
1900
1700
wavenumbers (cm−1)

FIG 1

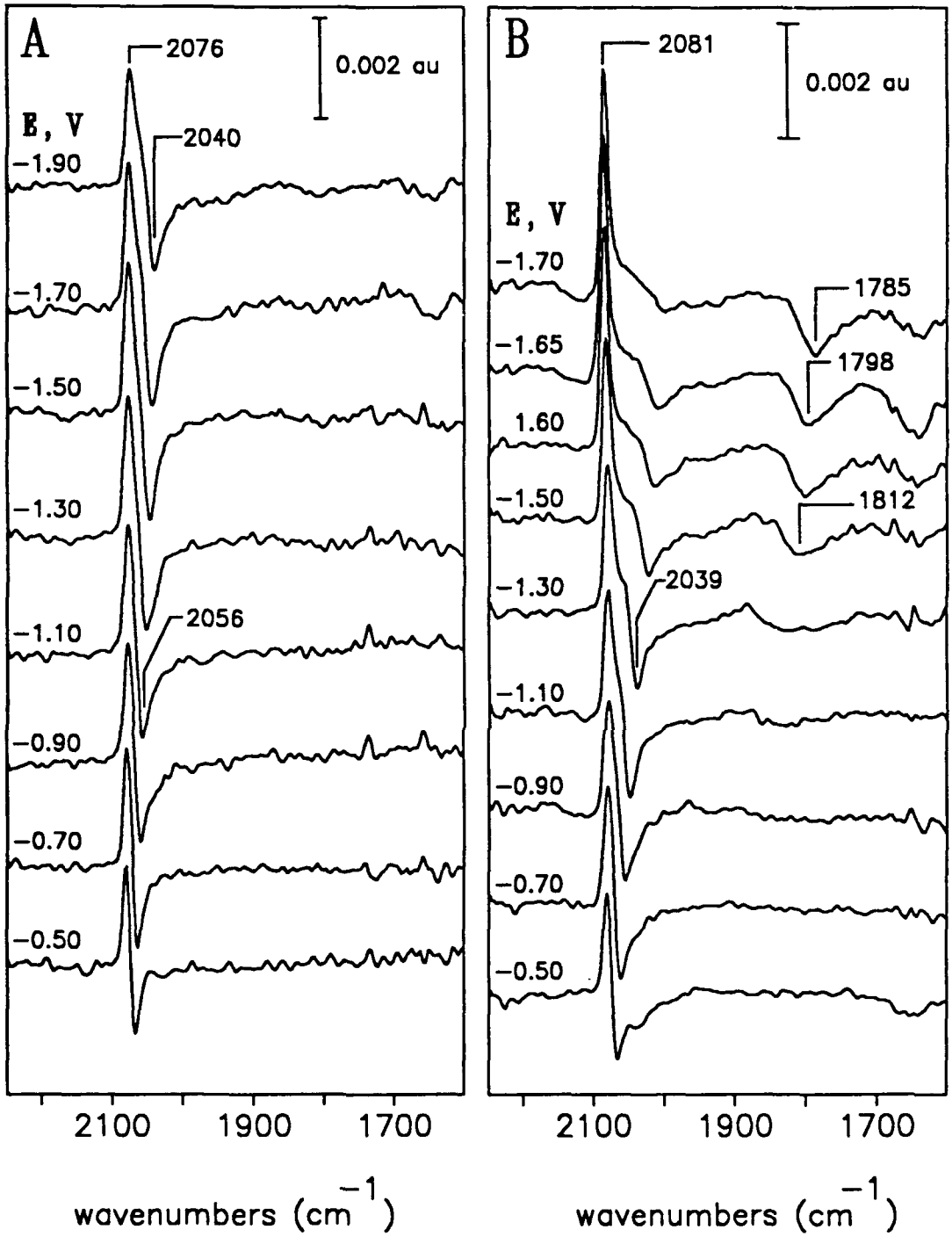
A
2076
0.002 au
E, V
2040
−1.90
−1.70
−1.50
−1.30
2056
−1.10
−0.90
−0.70
−0.50
2100
1900
1700
wavenumbers (cm−1)
B
2081
0.002 au
E, V
−1.70
1785
−1.65
1798
1.60
−1.50
1812
2039
−1.30
−1.10
−0.90
−0.70
−0.50
2100
1900
1700
wavenumbers (cm−1)

FIG 2

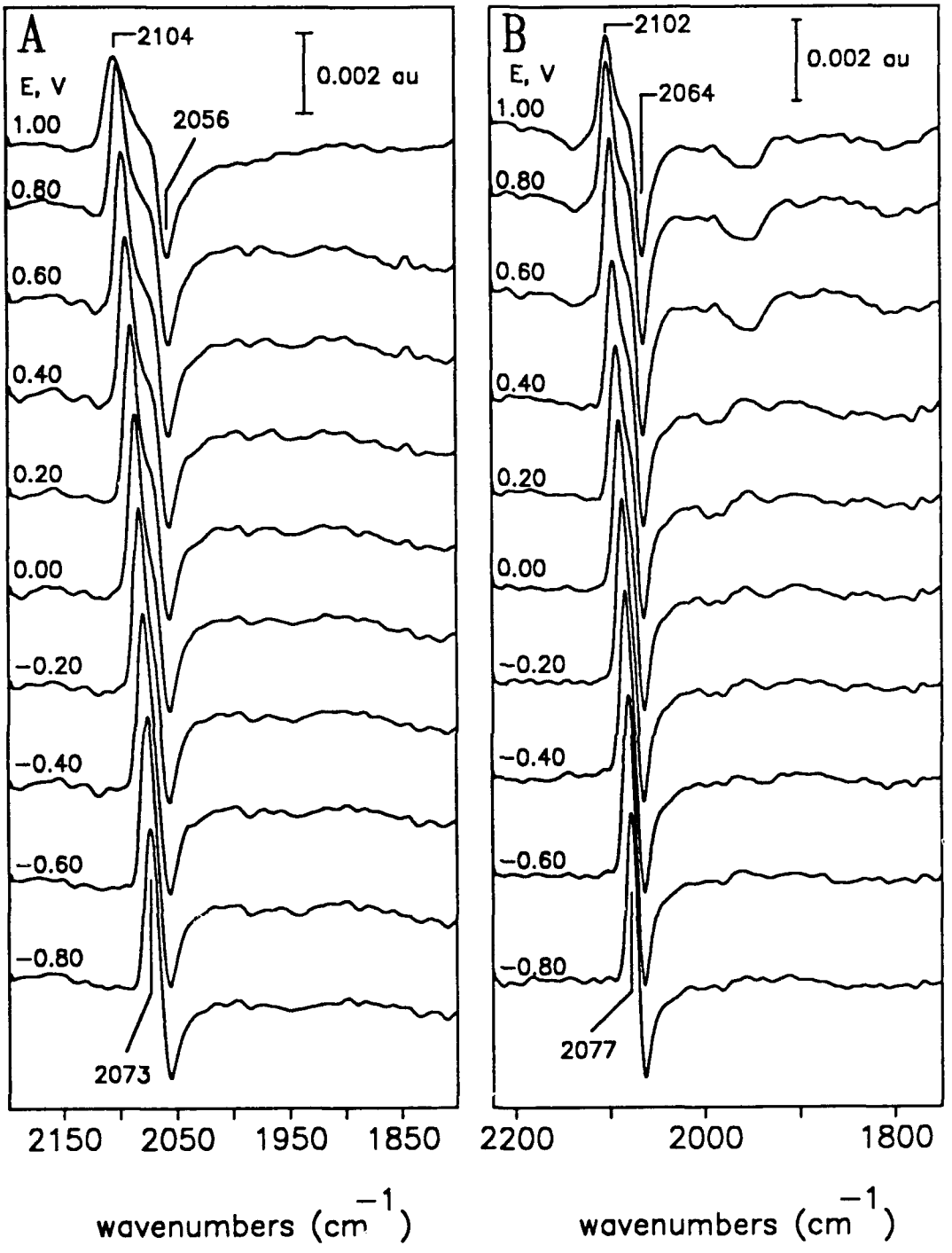
A
2104
2056
0.002 au
E, V
1.00
0.80
0.60
0.40
0.20
0.00
−0.20
−0.40
−0.60
−0.80
2073
2150
2050
1950
1850
wavenumbers (cm−1)
B
2102
2064
0.002 au
E, V
1.00
0.80
0.60
0.40
0.20
0.00
−0.20
−0.40
−0.60
−0.80
2077
2200
2000
1800
wavenumbers (cm−1)

FIG 3

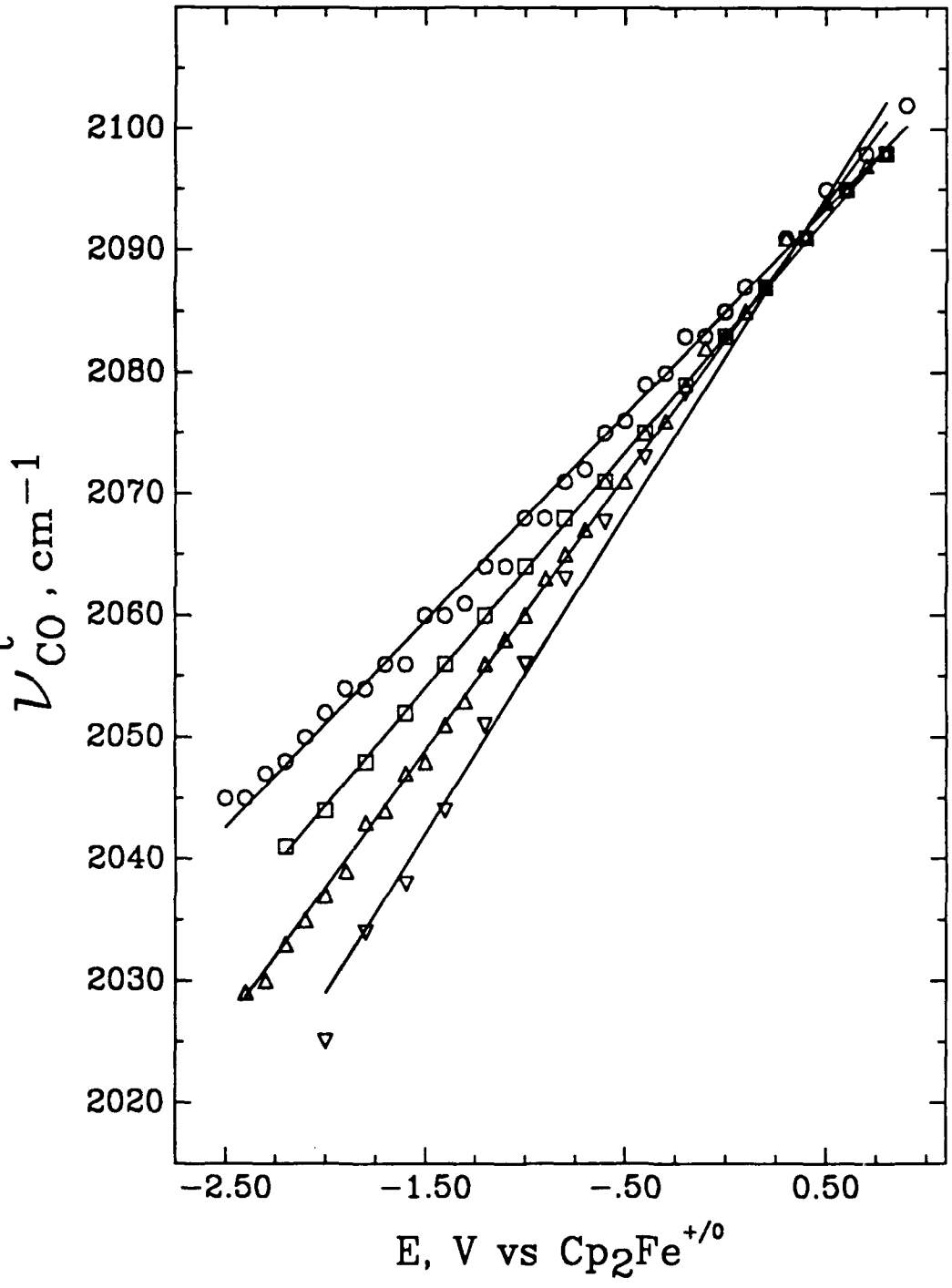
2100
2090
2080
2070
2060
2050
2040
2030
2020
ν^{t}_{CO}, cm^{-1}
−2.50
−1.50
−.50
0.50
E, V vs $Cp_2Fe^{+/0}$

FIG 4

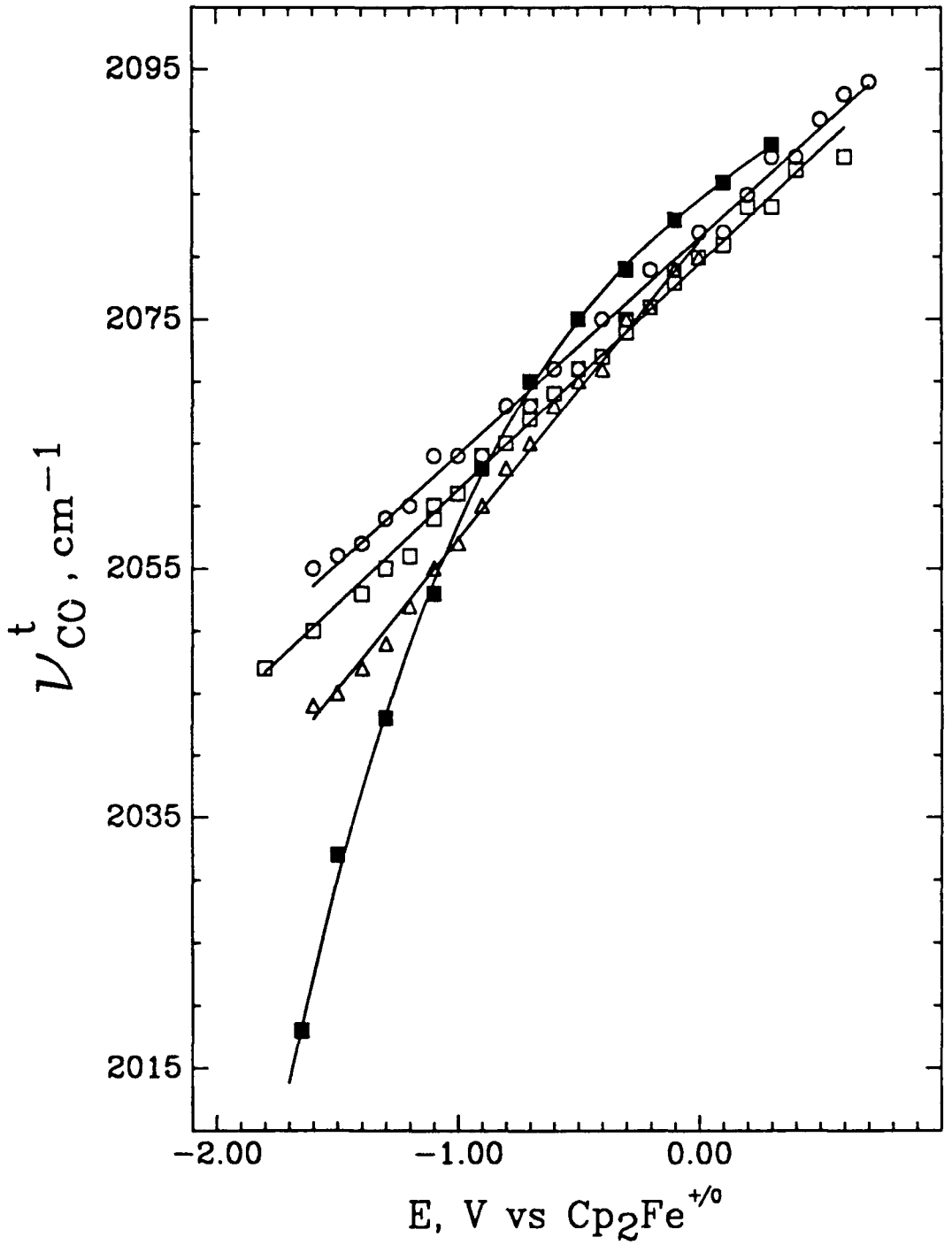

FIG 5

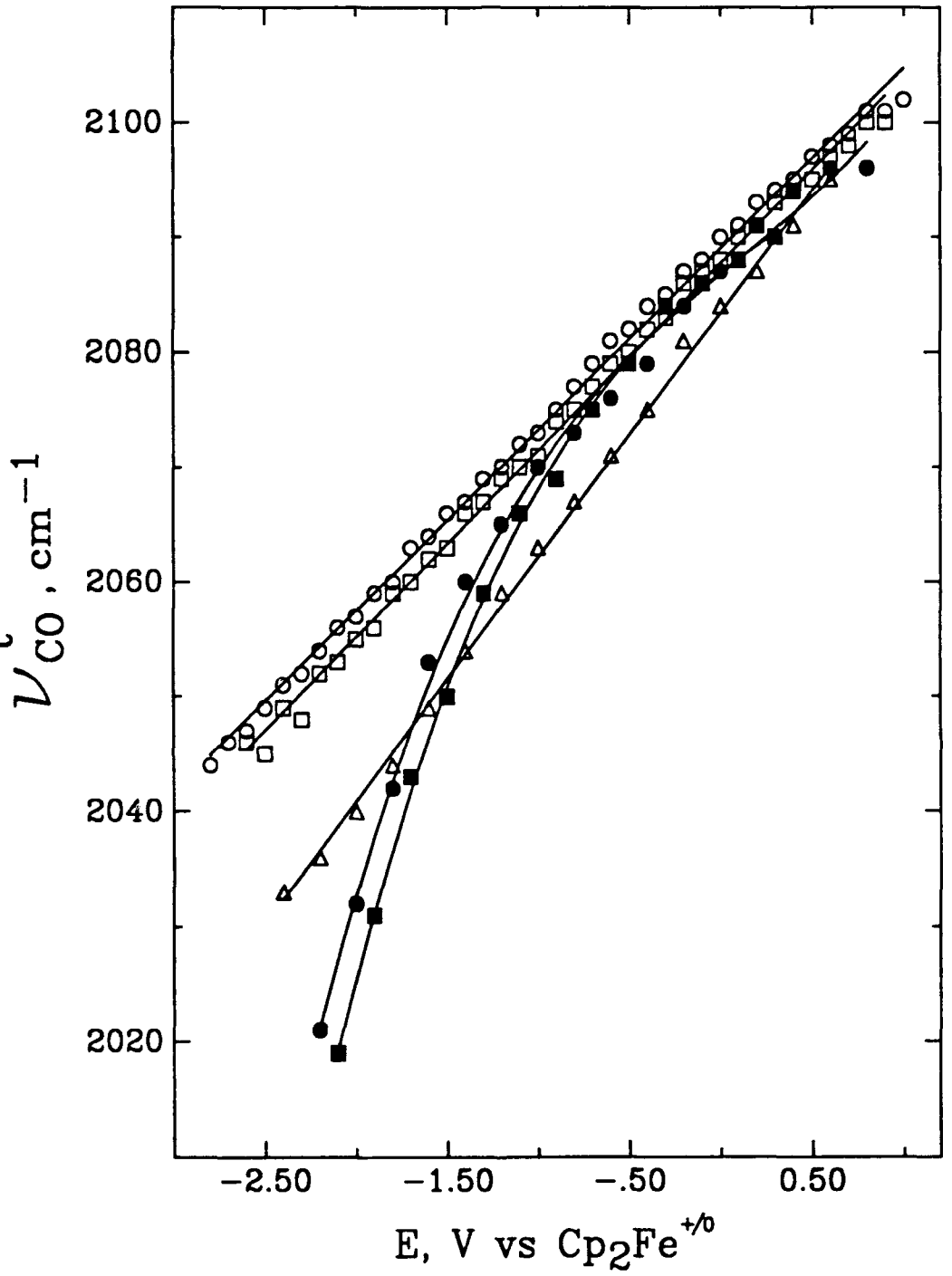

FIG 6

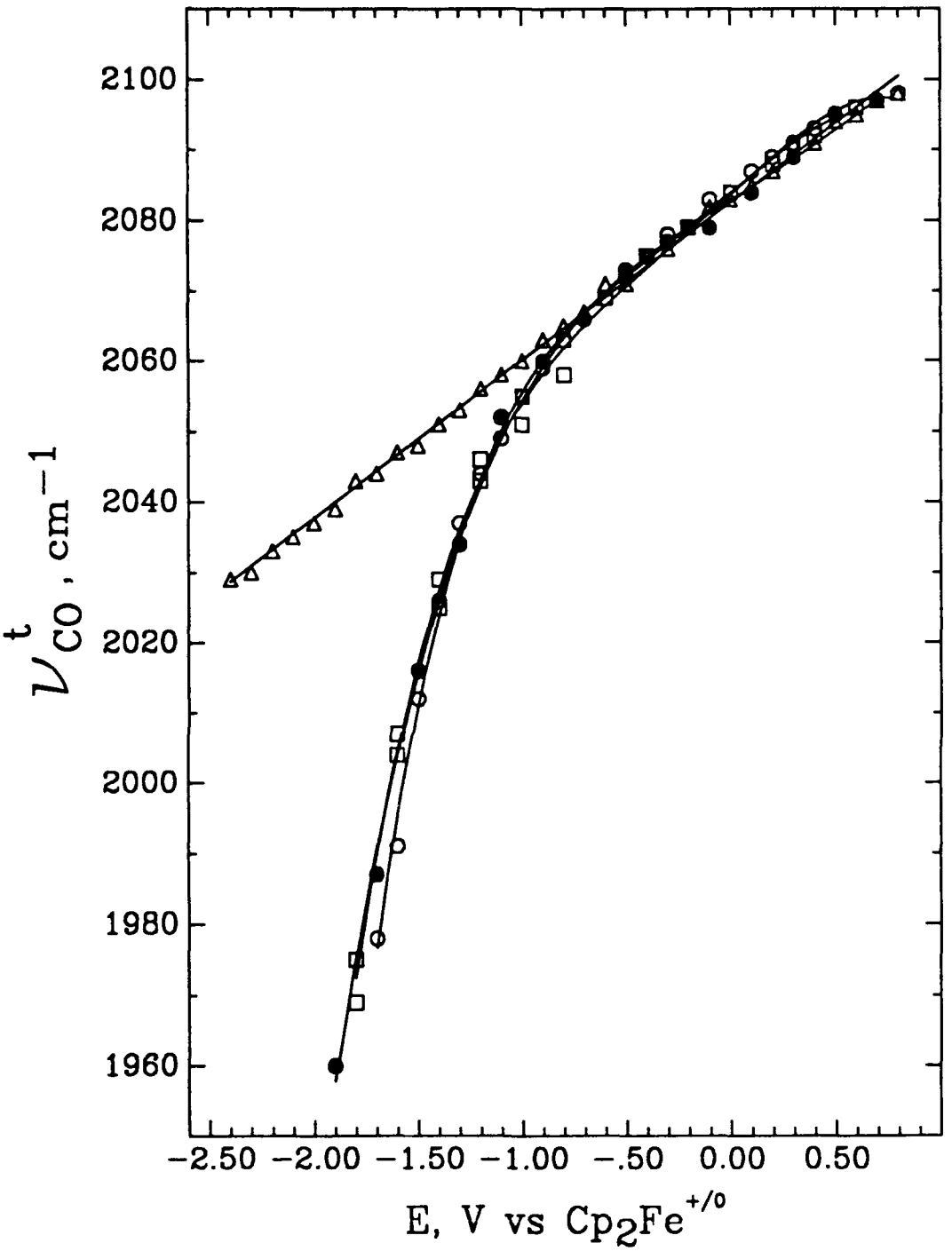
2100
2080
2060
2040
2020
2000
1980
1960
ν^{t}_{CO}, cm^{-1}
−2.50 −2.00 −1.50 −1.00 −.50 0.00 0.50
E, V vs $Cp_2Fe^{+/0}$

FIG 7

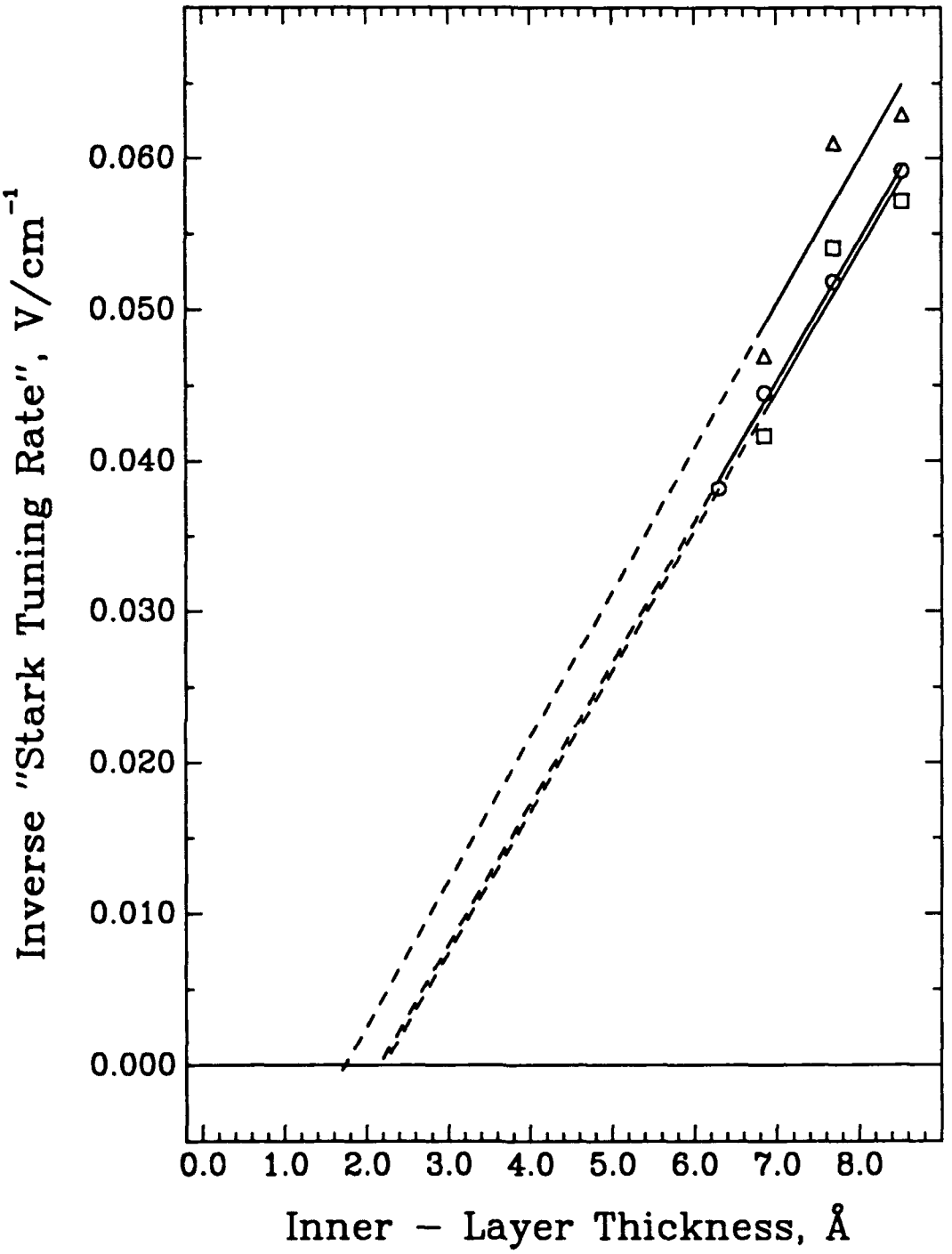
Inverse "Stark Tuning Rate", V/cm^{-1}
0.060
0.050
0.040
0.030
0.020
0.010
0.000
0.0
1.0
2.0
3.0
4.0
5.0
6.0
7.0
8.0
Inner – Layer Thickness, Å

FIG 8